Axial Magnetic Bearing Development for the BiVACOR Rotary BiVAD/TAH

Nicholas A. Greatrex*, Daniel L. Timms, Nobuyuki Kurita, Edward W. Palmer, and Toru Masuzawa

***Abstract*—A suspension system for the BiVACOR biventricular assist device (BiVAD) has been developed and tested. The device features two semi-open centrifugal impellers mounted on a common rotating hub. Flow balancing is achieved through the movement of the rotor in the axial direction. The rotor is suspended in the pump casings by an active magnetic suspension system in the axial direction and a passive hydrodynamic bearing in the radial direction. This paper investigates the axial movement capacity of the magnetic bearing system and the power consumption at various operating points. The force capacity of the passive hydrodynamic bearing is investigated using a viscous glycerol solution. Axial rotor movement in the range of $\pm$0.15 mm is confirmed and power consumption is under 15.5 W. The journal bearing is shown to stabilize the rotor in the radial direction at the required operating speed. Magnetic levitation is a viable suspension technique for the impeller of an artificial heart to improve device lifetime and reduce blood damage.**

***Index Terms*—Artificial biological organs, blood pumps, electromagnetic forces, magnetic levitation.**

I. Introduction

DUE TO the high rate of heart disease and a shortage of donor hearts, there has been interest in mechanical replacements for the heart for over 50 years. Unfortunately, these devices have had very limited success compared with traditional heart transplants, and their wide scale usage has been severely limited by their maintenance and performance drawbacks [1].

Mechanical circulatory devices have undergone a number of development stages. The first generation of ventricular assist devices (VADs) included pulsatile devices with pusher plates or flexing diaphragms and valve configurations [2]. These contacting components limited the device's life expectancy to less than 3 years [3]. The second generation of VADs used continuous flow rotary pumps with mechanical bearings and seals in contact with the blood [4], [5]. The smaller size of the second generation devices accelerated them to the forefront of VAD development; however, problems with the contact bearing systems still remain. Finally, the third and latest generation of VADs employ magnetic and hydrodynamic bearing systems to completely suspend the continuous flow rotor in the pump cavity [6]. By removing the need for contact bearing system, life expectancy of these devices can exceed 10 years.

Mechanical circulatory devices are designated as either total artificial hearts (TAH) or VADs [7]. In the case of TAHs, the patient's natural heart is removed and replaced with two mechanical pumps that provide perfusion to the systemic and pulmonary circulations. VADs are designed to supplement the output of the patient's natural left ventricle, but can also be used to aid the right ventricle or both ventricles simultaneously. In these three cases, the VAD is designated as an LVAD, RVAD, or BiVAD, respectively. The pumps that are used in VADs and TAHs are typically divided into two categories, pulsatile pumps and continuous flow pumps [8], [9]. As the names suggest, pulsatile pumps replicate the pulsing nature of the body's cardiovascular system, whereas continuous flow pumps produce a constant output flow from the device. The biggest advantages of the continuous flow devices are the increased mechanical reliability and thus reduced maintenance, as well as the device size [10].

Magnetic levitation and hydrodynamic bearings have recently been the focus of research for use in centrifugal VAD/TAH blood pumps, due to the significant advantage of reduced wear compared to traditional contact bearing systems [11].

BiVAD and TAH support is still dominated by pulsatile devices, whereas L-VAD development has moved toward third generation continuous flow devices. Currently, there are no continuous flow single unit BiVADs on the market or involved in trials. The third-generation BiVACOR BiVAD aims to treat end stage biventricular heart failure with a single rotary device.

The device, shown in Fig. 1, includes a set of left and right vanes positioned on rotating hub to form a double-sided centrifugal impeller. Active impeller suspension is achieved with an axial magnetic bearing and rotation via an electromagnetically coupled motor. Since the LVAD and RVAD impeller vanes are inherently coupled to the common rotation hub, changes in speed will alter the outflow of the left and right VADs. However, to account for required changes in instantaneous left/right outflow, the magnetic bearing system can displace the impeller axially within the pump cavity. This action simultaneously alters the efficiency of each semi-open impeller vane set in an inverse relationship. For example, a movement toward the left cavity will increase LVAD outflow while reducing RVAD outflow, and *vice versa*. The pump is designed to run at 2200 r/min

Manuscript received March 5, 2009; revised June 24, 2009. First published October 09, 2009; current version published February 17, 2010. *Asterisk indicates corresponding author.*

*N. A. Greatrex is with the Institute of Health and Biomedical Innovation, Queensland University of Technology, Brisbane, Qld. 4001, Australia (e-mail: n.greatrex@qut.edu.au).

D. L. Timms is with the The Helmholtz Institute, Rheinisch-Westfälische Technische Hochschule (RWTH), Aachen 52074, Germany (e-mail: timms@hia.rwth-aachen.de).

N. Kurita is with the Department of Electronic Engineering, Gunma University, Kiryu, Gunma 371-8510, Japan (e-mail: nkurita@el.gunma-u.ac.jp).

E. W. Palmer is with the Institute of Health and Biomedical Innovation, Queensland University of Technology, Brisbane, Qld. 4001, Australia (e-mail: e.palmer@qut.edu.au).

T. Masuzawa is with the Department of Mechanical Engineering, Ibaraki University, Hitachi, Ibaraki 310-8512, Japan (e-mail: masuzawa@mx.ibaraki.ac.jp).

Digital Object Identifier 10.1109/TBME.2009.2033389

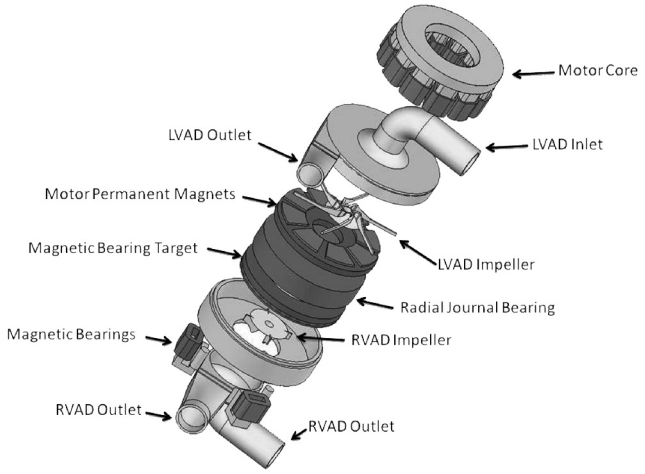

Fig. 1. Schematic of the BiVACOR device.

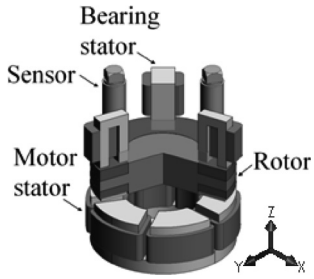

Fig. 2. Schematic of the magnetic motor-bearing system.

under normal physiological conditions; however, changes in the patients hemodynamics may require the pump to operate at speeds between 1700 and 2500 r/min. Preliminary investigations have shown that impeller movements of ± 0.2 mm in the BiVACOR can adequately alter the left and right pump flow for a wide range of hemodynamic conditions. The current prototype device is Ø 75 mm in diameter and 90 mm in length.

The objective of this paper was to investigate the stability of the rotor and determine the range of possible impeller axial movement, while maintaining suitable power consumption.

II. Materials and Methods

A. Identification of Hydraulic Forces

Determining the operating parameters and requirements for the magnetic bearing (MB) is a key step in the design process. In the case of the BiVACOR device, there are many hydraulic forces that act on the rotor when running in different conditions. An unbalanced axial force will develop in the BiVAD device as a result of the different pressure requirements of the left and right circulatory systems, as well as externally applied forces imposed on the impeller and pump encountered *in vivo*. The magnetic bearing system must be able to overcome these forces and stabilize the rotor in addition to proving the required torque.

To this end, a motor-shaft driven prototype device complete with force transducer (50M31, Jr3 Inc. Woodland, CA, USA) was inserted into a mock circulation loop [12] to measure the expected axial hydraulic force encountered by the impeller in pulsatile and nonpulsatile circulatory environments. The technique [13] can be used to determine the expected axial loads when operating the device in a BiVAD/TAH mode.

Furthermore, the torque requirements of the device should be calculated prior to design. Considering the VAD requires an output power of approx 1.33 W to provide normal hemodynamics to the systemic and pulmonary system, and assuming a device stage efficiency of $\sim$30%, the motor must generate 4.43 W. With a nominal rotational speed for this condition of 2500 r/min, the torque requirement of the motor is 0.017 N·m. However, higher torque values up to 0.04 N·m may be needed for elevated hemodynamic requirements.

B. Magnetic Bearing Design

Suspension of the rotor in the BiVACOR device is achieved by using an active magnetic suspension system in the axial direction and a passive hydraulic bearing in the radial direction. For use in a centrifugal pump, an axial bearing improves performance due to the ability to incorporate more magnetic material in the unused axial surface area of the impeller [14]. Karassik and McGuire state that bearing power is usually only needed for magnetic excitation of disturbance forces [15]. Incorporating permanent magnets into the magnetic bearing system, while using active electromagnets for fine control, can reduce power consumption. Fig. 2 shows the layout of the active axial magnetic suspension system. The prototype consists of the magnetic bearing, rotor, and motor.

A six-pole axial flux synchronous motor targets four permanent magnets placed on one side of the rotor. This motor provides torque to the rotor as well as a net axial attractive force. To counteract the axial force toward the motor, an active magnetic bearing is placed on the opposite side of the rotor. The magnetic bearing consists of three U shaped stators spaced evenly around the rotor. Custom Nb–Fe–B permanent magnets are embedded in the stator flux path to reduce the steady-state power required. The control coils are made of 276 turns of Ø 0.4 mm copper wire is wound around one leg of the stator. The flux generated by the control coil can be used to increase or decrease the flux produced by the permanent magnets. The magnetic bearing stators target an iron core embedded in the rotor.

The magnetic bearing system is designed to run at a steady-state condition where the electromagnetic coils are not excited and the force toward the bearings is generated only by the permanent magnets. The electromagnetic coils are used to stabilize the rotor in response to disturbances or to move the rotor to another position. Control of the active magnetic bearing is realized through PID controllers with position feedback. Additionally, potential difference (PD) control is also used for adjusting the amplitude of the motor's three phase sinusoidal drive signals. Position detection of the rotor is achieved by three eddy current sensors (U5B, Lion Precision, MN, USA) coupled to the magnetic bearing iron core target. Second-order low pass filters on the position sensor signal remove unwanted high frequency noise from the pulsewidth modulation (PWM) amplifiers. The

TABLE I
NOMENCLATURE

Symbol	Units	Description
$B_{R\,MAX}$	Wb·m^{-2}	The peak flux density of the rotor permanent magnets
$B_{S\,MAX}$	Wb·m^{-2}	The peak flux density of the stator
M		The pole pair number of the motor
ω	rad·s^{-1}	The rotating speed of the rotor
φ	rad	The phase difference
r_1	m	The inner radius of the rotor
r_2	m	The outer radius of the rotor
z	m	The equivalent distance of the air gap
μ_0	Wb·A^{-1}·m^{-1}	The permeability of vacuum
A	m^2	Cross sectional area of magnetic bearing stator
N	turns	Number of turns on MB stator
I_{eq}	A·t	The equivalent MMF of the MB permanent magnets
α	A·t·Wb^{-1}·m^{-1}	Constant relating to the geometry and thickness of MB permanent magnets
β	A·t·Wb^{-1}	Constant relating to the geometry and thickness of MB permanent magnets
i_{MB}	A	Current in the magnetic bearing control coil
i_{Motor}	A	Amplitude of the sinusoidal current in the motor coils

controller was designed and implemented using the dSPACE (DS1104, dSPACE, MI, USA) data acquisition system in conjunction with SIMULINK. Control output signals from dSPACE are fed through a linear current amplifier and then to the respective control and motor coils.

C. Magnetic Theory

Equations describing the theoretical magnetic force and torque generated by the magnetic components are derived using the virtual work method. It is assumed that the magnetic material is homogeneous and has a reluctance much smaller than that of the air gap. Axial attractive force and motor torque produced by the motor are given by (1) and (2). The axial force generated by the magnetic bearings is given by (3)

$$f_{z\mathrm{motor}} = \frac{\left(r_2^2 - r_1^2\right)\pi}{4\mu_0}\left[B_R^2 + 2B_R B_S\cos(\varphi) + B_S^2\right] \tag{1}$$

$$\tau_{z\mathrm{motor}} = \frac{zM\left(r_2^2 - r_1^2\right)\pi}{2\mu_0} B_R B_S \sin(M\varphi) \tag{2}$$

$$f_{z\mathrm{MB}} = -\frac{[Ni_{\mathrm{MB}} + I_{\mathrm{eq}}]^2}{\mu_0 A(\alpha z + \beta)^2}. \tag{3}$$

The parameters used in these equations are given in Table I. After identifying the operating requirements of the levitation system such as axial force and torque, an initial design point for the magnetic components can be determined from the theoretical equations. Values determined using this method for the winding number and component geometry are inflated to account for leakage flux, core saturation, variation in permanent magnet values and other characteristics which are not included or are estimated in the theoretical equations. Both the permanent magnet flux from the rotor and the flux generated by the motor coils are assumed to be sinusoidal and are described by

$$B_S(\theta, t) = B_{s\,\mathrm{MAX}}(i_{\mathrm{Motor}})\cos(\omega t - M\theta) \tag{4}$$

$$B_R(\theta, t) = B_{R\,\mathrm{MAX}}\cos(\omega t - M\theta - \varphi). \tag{5}$$

It is clear from (1) and (3) that by varying i_{MB} and i_{Motor} the axial forces on the rotor can be balanced against potential disturbance forces. Unbalanced forces over the face of the rotor can cause the rotor to tilt on the x and y axis. Fig. 3 demonstrates the principal behind tilt stabilization using the magnetic bearing system. The control flux generated by the electromagnetic coils is superimposed with the bias flux from the permanent magnets to create a flux density in the air gap. By changing the control currents to each magnetic bearing stator, different flux densities and forces can be generated by each stator. Tilt can then be correct for by reducing the force in the stator where the rotor is closest and increasing it where it is furthest away.

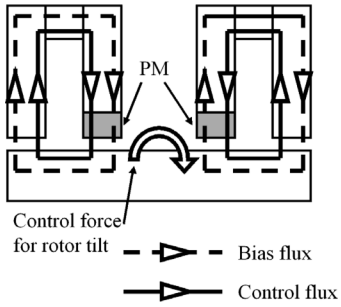

Fig. 3. Operation principle of the tilt control by the magnetic bearing.

D. FEM Analysis

Using the initial design parameters determined using the theoretical equations, 3-D models of the system components can be simulated in ANSYS to validate their performance characteristics. The 3-D finite element method (FEM) will be used to determine the magnetic field distribution in the system including, leakage flux and core saturation which was neglected from the analytical model due to the difficulties in determining these elements analytically. FEM analysis on the initial design returned that the force generated at the steady state operating point would be 15 N. The calculated flux distribution for this condition is shown in Fig. 4. At this ideal operating point, the electromagnets are not excited and the generated flux is only from the permanent magnets. FEM analysis was performed on the system at all expected operating points, such as maximum positive and negative coil current over the full range of rotor displacements. The analysis indicated that the magnetic materials does not saturate when operating at any of the device's operating points. A summary of the final design parameters for the magnetic components are shown in Table II.

E. Magnetic Force Characteristics

Due to the complicated nature of magnetic forces, experiments to determine the practical force characteristics were conducted on a specialized rig. These experiments were used to validate both the numerical and theoretical force results. A shaft

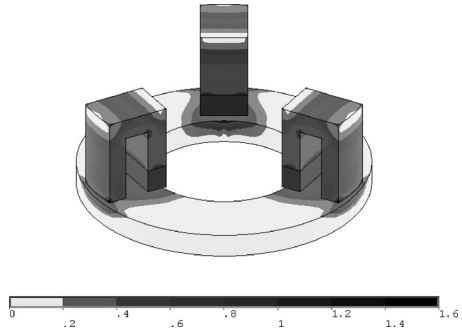

Fig. 4. Result of 3-D FEM analysis on the magnetic bearings.

TABLE II
PARAMETERS OF PROTOTYPE

Parameter	Value
Bearing (S45C Iron)	
Stator height	21.5 mm
Coil turns (wire Ø 0.4mm)	276 turns/pole
PM flux density	N45
PM thickness	3 mm
Motor (S45C Iron)	
Stator height	10 mm
Coil turns (wire Ø 0.4 mm)	180 mm
PM thickness	1 mm
Rotor (Disc: S45C, Core: POM)	
Outer diameter	Ø 49 mm
Inner diameter	Ø 27 mm
Thickness (bearing side)	2 mm
(motor side)	2 mm
(core)	8 mm

Specifications of the motor, magnetic bearing, and rotor.

with radial bearings was attached to the rotor to restrict it in the radial direction. A micrometer connected in the axial direction was used to fix the rotor to a defined axial clearance. A force transducer measured the axial force acting on the rotor from the bearing and motor at various operating conditions. The rotor was moved throughout its expected range of ± 0.2 mm and the magnetic excitation currents were varied from -3 to $+3$ A for the bearing and from 0 to 3A for the motor.

F. Levitation Performance and Stability

The primary objective of the study was to determine if stable levitation of the rotor can be achieved in both the radial and axial direction. Additionally, the research also ascertained the movement and operating limits of the rotor in the axial direction using the magnetic bearing.

Initially, the rotor was levitated without rotation. Once stable levitation is achieved, the rotor was accelerated up to a speed of 2500 r/min. At the identified operating point of 2500 r/min, the rotor was moved axially using the active magnetic bearing. Finally, the dynamic response of the system was determined from step inputs to the control system.

Radial stability of the rotor is achieved passively with a short plain hydrodynamic journal bearing shown in Fig. 1. The journal bearing requires a fluid medium to be effective. As such, to determine the stabilizing effect of the journal bearing, the experiments were run twice, once in air and once in a 38%/62% wt. Glycerol/water mixture, which has a viscosity similar to blood.

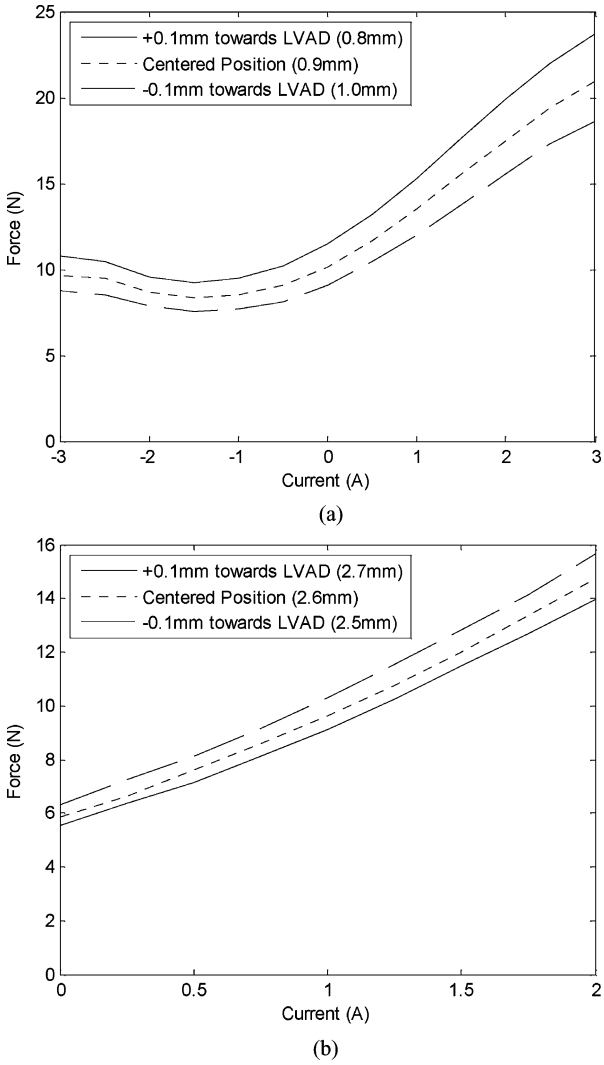

Fig. 5. (a) Measured magnetic bearing axial force. (b) Measured motor axial attractive force.

III. EXPERIMENTAL RESULTS

A. Mock Loop

Operating the shaft mounted BiVAD impeller while connected to the circulation loop replicating pulsatile biventricular heart failure produced a maximum impulse force of 12 N. Removing heart pulsatility from the loop, and thus simulating total biventricular heart failure, a maximum force of 3 N was produced. This force reduced as impeller position was altered from the central position.

B. Force Measurement

Magnetic force measurements with varying axial air gaps and excitation current were recorded for the levitation system, with results for bearing and motor attraction displayed in Fig. 5(a) and (b). The figures show superimposed curves for three

different rotor displacements. The absolute air gaps of the bearing and motor to the respective faces of the rotor are given in parentheses in the legend. When the rotor is operating at the center of the pump casing the absolute distance from the ferromagnetic material to the bearing and motor face is 0.9 and 2.6 mm, respectively. The force generated at these points is indicated by the dashed line. As expected the force increases as the separation distance between the components decreases as indicated by the solid and long-dashed lines.

The three bearing stators produced a combined force of 10 N at zero current and a magnetic air gap of 0.9 mm. A current stiffness of 3.6 N/A was produced for positive flowing current, however this reduced significantly with negative current, due to the inability for the active magnetic flux to efficiently cancel the permanent magnetic flux. A minimum force turning point was observed at -1.5 A. This value will be set in the control system as the minimum current to ensure that the forces do not increase by moving past the turning point.

With an additional rotor weight of 1 N, the motor stator produced a balancing attractive force of 9 N at 2.5 mm air gap, with 1 A current. A constant 1 A bias current was considered essential to produce sufficient torque for rotation when required. The current stiffness for positive current at this position was 5 N/A.

From the results, it was observed that the force generated is a nonlinear function of both rotor displacement and excitation current. This observation is in agreement with both derived theoretical formulas and the FEM analysis.

C. Levitation

Initially, the rotor was levitated successfully without rotation. The parameters for the bearing PID controller and the motor PD controller were determined manually through trial and error. Once levitation was achieved, the control parameters were manually tuned to achieve appropriate rise times, overshoot, settling time, and steady-state error. The parameters for the system were $K_p = 14$ A/mm, $K_i = 20$ A/mm/s, and $K_d = 0.06$ A·s/mm. The rotation and dynamic controller tests were then performed in Air and the Glycerol mix.

D. Dynamic Characteristics

Fig. 6(a) and (b) shows the rotor response to a 0.28 mm step input at 2200 r/min in air and glycerol, respectively. The rotor was initially offset by -0.14 mm from the center position to allow a large step movement of the rotor in the test. Fig. 6(a) shows the rotor movement in response to the 0.28 mm step input. The response exhibits overshoot and a 2 s settling time. In Fig. 6(b), it is clear that the glycerol mixture has had a big effect on the system dynamics. Increased damping due to the viscous fluid resulted in longer rise and settling times to the same step input. The rise time and settling time for the glycerol experiment was 0.8 and 5 s, respectively.

E. Levitated Rotation Characteristics

The rotor was accelerated up to 2500 r/min in both air and glycerol mixture. Fig. 7 shows the amplitude of the axial vibration of the rotor at each rotational speed for air and glycerol. The vibrations were reduced significantly at all speeds when glycerol was used.

Radial sensors were used to measure the displacement of the rotor along the x and y axis. Fig. 8 shows the movement of the rotor in the radial directions at 2200 r/min. The dashed line represents the physical extremities of the radial movement. When only air is present in the pump, the radial movement is quite significant and it can be seen that the rotor touches down a number of times. However, when running in glycerol, no radial

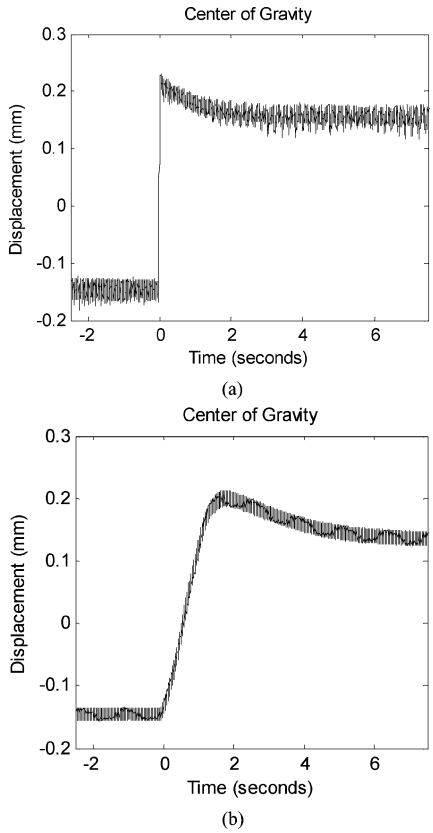

Fig. 6. (a) Step response of 0.28 mm in air at 2200 r/min. (b) Step response of 0.28 mm in glycerol at 2200 r/min.

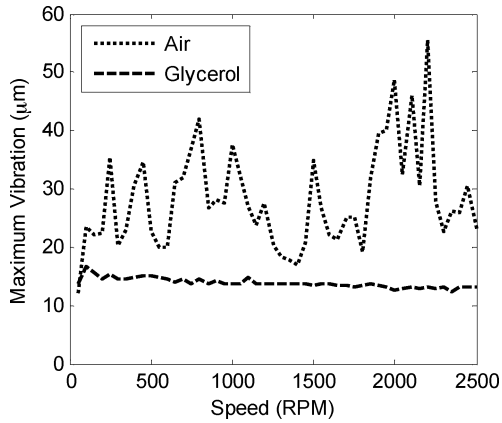

Fig. 7. Amplitude of axial vibration at different rotational speeds.

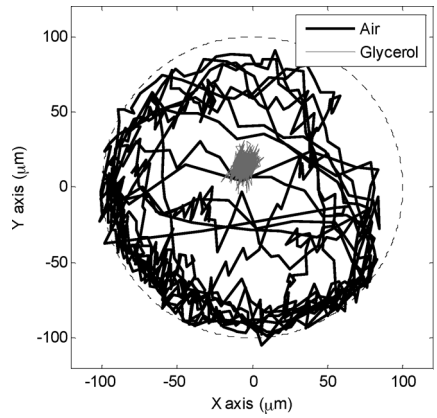

Fig. 8. Comparison of radial rotor movement in air and glycerol at 2200 r/min.

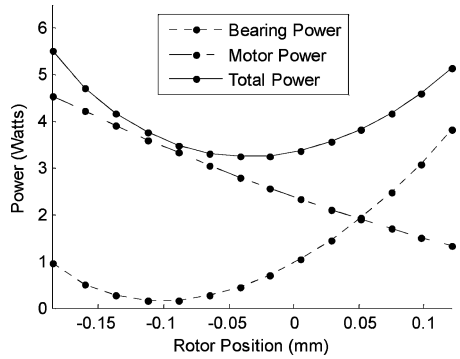

Fig. 9. Motor-bearing power consumption for movement of the rotor in the axial direction at 0 r/min in air.

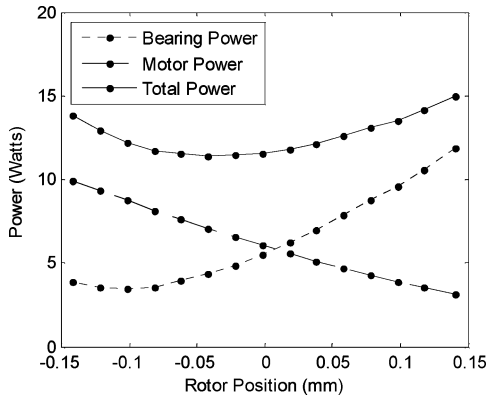

Fig. 10. Motor-bearing power consumption for movement of the rotor in the axial direction at 2200 r/min in glycerol.

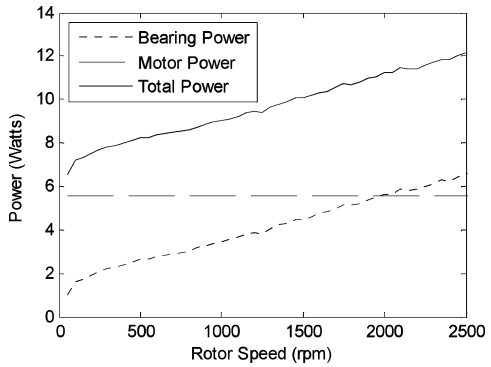

Fig. 11. Motor-bearing power consumption at 0 mm for increasing rotational speeds in glycerol.

touchdown was observed and the radial movement was confined to a small region. Similar observations were made for the range of speeds from 1700 to 2500 r/min.

F. Power Consumption

Axial movement of the rotor was achieved for displacements of ± 0.15 mm. Initially the rotor was levitated in air without rotation. Fig. 9 shows the power consumption of the device under these conditions. The parabolic power consumption function is a product of the two proportional feedback controllers for the bearing and motor. The minimum total power point was at -0.05 mm.

Fig. 10 shows the power consumed by the bearing and motor components as well as the total power used for various rotor displacements at 2200 r/min in glycerol. The control parameters and motor amplitude were modified for the glycerol case to increase stability. For movement of ± 0.15 mm the power total power consumption was less than 15 W at 2200 r/min.

Changes in power consumption as the rotor accelerates are shown in Fig. 11. The rotor was stabilized in the center position and the rotational speed was increased to 2500 r/min. The motor power consumption stayed constant throughout the experiment because the position of the rotor was stable at 0 mm. In the central position at 2200 r/min, the power consumption was approximately 11.5 W.

IV. Discussion

Magnetic levitation is a viable suspension technique for the impeller of an artificial heart to improve device lifetime and reduce blood damage. In the implantable blood pump application, the magnetic bearing must counter disturbing forces due to the hydraulic pressure developed within the pumping chamber. Precise determination of these loads must be specified in order to complete the bearing design [16].

The theoretical magnetic flux required for sufficient force generation in the motor and bearing stators was calculated using these hydraulic forces as design criteria. However, although these equations allow the initial geometric design of the magnetic components, it is well known that these equations overestimate the actual force production capacity of a magnetic system due to the lack of simulated flux path leakage and nonlinear permeability of the iron core. Therefore, finite element methods are frequently used to predict the force generation performance of such systems.

Following simulation, the model must be validated with practical measurements. In this case, the prototype magnetic bearing produced a 10 N force at a 0.9 mm air gap. This value was lower than the simulated value of 15 N due to inaccuracies with the permanent magnet and material properties of the model. Further refinement of the simulation will be conducted in the future to yield more accurate results. Motor force measurements were

conducted with the motor air gap of 2.5 mm when 1 A of current was supplied to the motor coils and the rotor weight was directed toward the motor stator. This static value of offset motor current was included to provide sufficient rotational torque to enable levitated rotation to the desired speed of 2500 r/min.

A prototype device was constructed which featured a ± 0.2 mm clearance gap between the rotor and pump cavity housing. Using the measured force characteristics, appropriate spacing of 0.9 and 2.5 mm between the rotor and the bearing and motor components, respectively, were used to ensure the magnetic zero point was positioned close to the geometric center point. The magnetic levitation system will be designed to operate around this point to minimize the power used to levitate the rotor under normal operating conditions. However, due to discrepancies in the operating force characteristics, the magnetic zero point in the developed prototype was located 0.1 mm away from the geometric center point at 2500 r/min.

In the final pump design, impeller blades will be affixed above the permanent magnets. This effectively increases the separation between the motor and the rotor. The large air gaps used in this prototype include the allowances for the future impeller blades. Additionally, the larger gaps between the magnetic actuators and the rotor ensure that the magnetic characteristics of the system do not change rapidly with small rotor displacements.

Additional force measurements revealed that both the motor and bearing could produce sufficient balancing force when the impeller was moved off the centralized position. For example, a movement of 0.1 mm toward the motor reduced the air gap to 2.5 mm, and thus increased its attractive force to 10.3 N. This required the supply of $+0.75$ A to the bearing, now operating with an air gap of 1.0 mm, to produce a 11.3 N balancing force. Likewise, a movement of 0.1 mm toward the bearing required -0.5 A current supply to each bearing coil to partially cancel the phase modulation (PM) flux and balance the force.

The force results exhibited nonlinear force characteristics dependent on both current and displacement. When the rotor is operating close to the magnetic bearings, the force generated by the permanent magnets must be reduced by reversing the coil current to cancel the bias flux. However, it can be seen that even at the point of minimum force, a small force is still generated. This is due to the coil flux not completely canceling the permanent magnet flux due to significant leakage flux. This phenomenon was confirmed with both finite element software and empirical results. Further design iterations will seek to reduce this problem and allow for greater cancellation of the bias flux.

Experiments in both air and glycerol were conducted to determine the effectiveness of the hydrodynamic journal bearing to stabilize the rotor in the radial direction. The experiments demonstrated that when running in glycerol and at the required operating speed range of 1700–2500 r/min, the rotor was stabilized with a small eccentricity ratio near the center of the case. Stable movement of the rotor using the axial magnetic levitation system was restricted to ± 0.15 mm due to vibration and insufficient force generation when operating more than 0.15 mm away from the center. This is less than the ± 0.2 mm movement that was proposed in the design criteria. Modification of both the magnetic components and control system in future prototypes will improve the movement range.

The presence of the viscous fluid glycerol had a drastic effect on the performance of the magnetic bearing system. In particular, the dampening characteristics of the system were significantly increased. The high level of damping was principally due to the small clearances in the pump case. Axial movements of the rotor required the shifting of the fluid from one side of the rotor to the other via the thin journal bearing gap. It is expected that the amount of dampening present in the pump will decrease in the final design due to the easy movement of the fluid through the inlet and outlet ports of the pump.

The performance of the levitation system was sufficient to maintain stable levitation and rotation at speeds required for BiVAD support. As was expected, power consumption for the bearings increased as the rotor moved toward the motor and was decreased when close to the bearings. The motor sinusoidal amplitude was dependent on a proportional feedback controller and as such increased and decreased as the rotor position changed. These two inverse power characteristics combine to form a total power function that has a minimum and two monotonically increasing asymptotes. A worst case no load power consumption was recorded at approximately 15 W, which was more than the target 10 W. A target of 10 W is desirable to limit excessive heating of surrounding tissue and blood, as well as enhance battery lifetime between charges.

In addition to the changes in power consumption for axial movement, rotational speed changes also brought about a significant increase in power consumption. This increase can be attributed to the changes in the magnetic force characteristic of the motor as the speed increases, as well as power required for the suppression of vibrations.

Reduction of the power consumption at the operating speed will be achieved by utilizing optimized nonlinear control systems as well as optimizing the magnetic bearing and motor geometry to perform most efficiently at required operating speed range.

V. Conclusion

An axial magnetic motor-bearing rig was designed and constructed, and suspension characteristics of the system evaluated for use in an implantable BiVAD. Total magnetic bearing and motor power was below 15 W for an axial displacement of ± 0.15 mm and rotational speed of 2200 r/min. According to the step response, rotor vibration stabilized after a step input of 0.28 mm, which demonstrates stable control performance. Radial stability of the rotor by the hydrodynamic journal bearing was confirmed in glycerol. Additionally axial vibrations were shown to be reduced significantly in the presence of the glycerol solution.

Acknowledgment

The authors would like to thank QUT workshop, Brisbane, Australia, MNCT workshop, Miyakonojo, Japan and Helmholtz Institute Workshop, Aachen, Germany for their help and support.

REFERENCES

[1] T. Akamatsu, T. Nakazeki, and H. Itoh, "Centrifugal blood pump with a magnetically suspended impeller," *Artif. Organs*, vol. 16, no. 3, pp. 305–308, 1992.

[2] D. Olsen, "Rotary blood pumps: A new horizon," *Artif. Organs*, vol. 23, no. 8, pp. 695–696, 1999.

[3] E. H. Maslen *et al.*, "Artificial hearts," in *Proc. 1997 IEEE Int. Conf. Control Appl.*, 1997, pp. 204–209.

[4] H. G. Wood *et al.*, "The medical physics of ventricular assist devices," *Rep. Progr. Phys.*, vol. 68, pp. 545–576, 2005.

[5] R. K. Jarvik, "System considerations favouring rotary artificial hearts with blood-immersed bearings," *Artif. Organs*, vol. 19, no. 7, pp. 565–570, 1995.

[6] H. Hoshi *et al.*, "Magnetically suspended centrifugal blood pump with a radial magnetic driver," *ASAIO J.*, vol. 51, no. 1, pp. 60–64, 2005.

[7] P. L. DiGiorgi *et al.*, "Which patient, which pump?" *J. Heart Lung Transplant.*, vol. 22, no. 3, pp. 221–235, 2003.

[8] S. G. Drakos *et al.*, "Comparison of pulsatile with nonpulsatile mechanical support in a porcine model of profound cardiogenic shock," *ASAIO J. (Amer. Soc. Artif. Internal Organs, 1992)*, vol. 51, no. 1, pp. 26–29, 2005.

[9] W. J. Weiss, "Pulsatile pediatric ventricular assist devices," *ASAIO J. (Amer. Soc. Artif. Internal Organs: 1992)*, vol. 51, no. 5, pp. 540–545, 2005.

[10] K. X. Qian *et al.*, "Toward a durable impeller pump with mechanical bearings," *ASAIO J.*, vol. 48, no. 3, pp. 290–292, 2002.

[11] R. Wampler *et al.*, "A sealess centrifugal blood pump with passive magnetic and hydrodynamic bearings," *Artif. Organs*, vol. 23, no. 8, pp. 780–784, 1999.

[12] D. L. Timms *et al.*, "A complete mock circulation loop for the evaluation of left-, right-, and bi-ventricular assist devices," *Artif. Organs*, vol. 29, no. 7, pp. 564–571, 2005.

[13] D. L. Timms *et al.*, "LVAD pump performance and force characteristics in a pulsatile complete mock circulation loop," *Artif. Organs*, vol. 29, no. 7, pp. 572–580, 2005.

[14] T. Masuzawa *et al.*, "Magnetically suspended centrifugal blood pump with an axially levitated motor," *Artif. Organs*, vol. 27, no. 7, pp. 631–638, 2003.

[15] I. J. Karassik *et al.*, *Pump Handbook*, 3rd ed. New York: McGraw-Hill, 2000.

[16] D. Japikse, W. Marscher, and R. Furst, *Centrifugal Pump Design and Performance*. Vermont: Concepts ETI, 1997.

Authors' photographs and biographies not available at the time of publication.